Int. J. Electrochem. Sci., 16 **(2021)** Article Number: 211031, doi: 10.20964/2021.10.40

International Journal of
ELECTROCHEMICAL
SCIENCE
www.electrochemsci.org

Ipomoea batatas leaves extract as a green corrosion inhibitor for Q235 steel in HCl solution

Wenguang Zeng [1,2], *Yanyan Xu* [1,2], *Pengli Ge* [1,2], *Wenwen Xiao* [1,2], *Qingshan Liu* [1,2], *Zhengyuan Gao*[3,*], *Yongbo Yan*[4,*],

[1] SINOPEC Northwest Company of China Petroleum and Chemical Corporation, Urumqi 830011, China;
[2] Key Laboratory of Enhanced Oil Recovery in Carbonate Fractured-vuggy Reservoirs, SINOPEC, Urumqi 830011, China
[3] School of Mechatronics & Vehicle Engineering, Chongqing Jiaotong University, Chongqing, 400074, China;
[4] School of Oil and Natural Gas Engineering, Southwest Petroleum University, Chengdu 610500
[*]E-mail: zhengyuangao@cqjtu.edu.cn (Z. Gao); 779265488@qq.com (Y. Yan).

Received: 30 June 2021 / *Accepted:* 2 August 2021 / *Published:* 10 September 2021

In this study, *Ipomoea batatas* leaves extract (IBLE) was prepared to control Q235 steel corrosion in 1 M HCl solution firstly. The adsorption and corrosion inhibition properties were examined by weight loss, surface topography and electrochemical methods, as well as theoretical simulations. Experimental results reveal that IBLE is a high efficiency mixed-type inhibitor with optimal performance of 96.4% at 200 mg/L. This contributes to the adsorption of IBLE onto steel samples, which involves both physisorption and chemisorption, consequently forming a strong protective film between steel and acid solution. In addition, molecular simulation results further confirm that IBLE can be effectively adsorbed onto Fe(110) substrate. Therefore, we developed a novel eco-friendly, efficient corrosion inhibitor for steel in HCl solution.

Keywords: Corrosion inhibitor; Extract; DFT; Langmuir; Molecular dynamics simulation.

1. INTRODUCTION

The acid pickling process is commonly used to remove the undesired scales, oxides and other contaminations from metal surface like mild steel [1-3]. Strong acids like sulfuric acid or hydrochloric acid have been frequently utilized for this purpose, which can bring severe metal dissolution during acid treatment. In order to solve this problem, introducing specific amounts of corrosion inhibitors to the aggressive solution is a common way [4]. Despite the high inhibition efficiency of various organic

inhibitors, most of them are harmful for the ecosystem and human health. Therefore, the development of eco-friendly and cost-effective corrosion inhibitors such as drugs [5, 6], nanomaterials [7, 8], ionic liquids [9-11], and plant extracts[12-15] have attracted more and more attention of researchers in corrosion field. Among them, the plants extract is considered as the most promising and suitable candidates to conventional toxic inhibitors owing to the natural, renewable, easy to access, and high efficient properties.

The plant extracts consist of various complex compounds, including tannins, flavonoids, alkaloids, phenolics, nitrogen bases, amino acids, and so on [16, 17]. It is found that these natural organic compounds are full of heteroatoms and polar functional groups, which could act as adsorption centres to the metallic surface [18]. As a result, these compounds can form protective layer to retard the metal corrosion process against acidic electrolytes. Many plants extract as green corrosion inhibitors have been developed in recent years [19-23]. Alvarez et al. evaluated the inhibition ability of *Rollinia occidentalis* extract for steel corrosion in HCl solution, and found that this extract can be used as an efficient mixed-type inhibitor [24]. Qiang et al. explored the adsorption and inhibition mechanism of *Ginkgo* leaf extract on X70 steel in HCl by various experimental and theoretical methods [13]. The obtained superior inhibition capacity was attributed to the adsorption of its various organic constituents on X70 steel, forming a ordered protective film towards corrosive attack. Besides, the computational modeling results confirmed the inhibitor adsorption on steel surface through its active centres. The corrosion inhibition of mild steel in 1 M HCl containing *Mango* leaves extract was examined by Ramezanzadeh and co-authors [25]. Results showed a mixed inhibition action of this extract, which decreased both iron anodic dissolution and cathodic hydrogen evolution efficiently.

In addition, *Ipomoea batatas* are widely distributed in Asia, America and Europe. Therefore, the use of *Ipomoea batatas* leaves extract (IBLE) as the corrosion inhibitor has numerous sources. In present study, the water extract of *Ipomoea batatas* leaves as an green corrosion inhibitor of Q235 steel in 1 M hydrochloric acid was explored via weight loss, electrochemical, surface morphology methods and computational modeling. These experimental and computational results synergistically prove that IBLE can provide inhibition ability for steel in HCl availably. Meanwhile, the interaction mechanism between IBLE and steel was explored and analyzed at the molecular/atomic level. This work will give important guidance for designing and developing novel green corrosion inhibitors.

2. EXPERIMENTAL

2.1. Preparation of IBLE

The *Ipomoea batatas* was collected and washed with deionized water. At first, it was dried at 323 K for two days in an air dry oven. Next, it was smashed to powder by a pulverizer followed by deionized water extraction for 6 h. After the extraction, the filtrate was dried by spin steaming instrument followed with freeze-dried for 48 h to obtain the IBLE powder. Finally, the powder was put into a desiccator for later use.

2.2. Electrodes and solutions

Q235 steel was cut into 1 cm^3 samples and sealed with epoxy resin, remaining 1 cm^2 surface for working electrode in the electrochemical test. The corrosive solution was 1 M HCl, prepared by concentrated hydrochloric acid with deionized water. The used concentration of IBLE were 50, 100, 150, 200 mg/L, respectively, while the solution without IBLE was treated as blank. For each test, both the newly polished steel samples and fresh solution were used.

2.3. Electrochemical measurements

A conventional three-electrode cell was used to evaluated the electrochemical tests via CHI 760E station. This measurement cell contains the steel working electrode, counter electrode (platinum sheet), and reference electrode (saturated calomel electrode). Firstly, the working electrode was immersed in corrosive solution to obtain a stable state. The open circuit potential (E_{OCP}) was recorded meanwhile. The EIS test was then introduced using 5 mV/s sinusoidal wave versus E_{OCP} with frequency scope of 10^5–10^{-2} Hz. Finally, the potentiodynamic polarization (PDP) test was performed within ±250 mV potential range based on E_{OCP}. The corresponding scan rate was 1 mV/s. The test environment was controlled at 298 K.

2.4. Gravimetric method

Steel samples used for the weight loss was ultrasonically cleaned with deionized water and ethyl alcohol, rapidly dried, and weighted. After that, the steel specimens were immersed in corrosive media containing various concentrations of IBLE for 6 h. Thereafter, the samples were washed by deionized water and ethanol, dried, and weighed again. The same experiment was triplicate to reduce personal error.

2.5. Surface observation

SEM (Scanning Electron Microscopy, FEI Quanta FEG 250, USA) and LSCM (Laser Scanning Confocal Microscopy, LSM700, Germany) were employed to observe the surface morphologies of steel samples immersed in 1 M HCl with and without 200 mg/L IBLE at 298 K. The immersion time of specimens used for SEM and LSCM were 4 h and 1 h, respectively.

2.6. Computational calculation

Based on the main constituents (2-amino-5-guanidinopentanoic acid, AGA; 2-amino-3-phenylpropanoic acid, APA; dodecanoic acid, DA; 2-amino-3-(1H-imidazol-4-yl)propanoic acid, AIA, which are shown in Fig. 1) of IBLE, we performed the molecular modeling methods including DFT calculation and molecular dynamics (MD) simulation to get insights to corresponding interaction

mechanism. The active centres of main IBLE constituents were explored by DFT calculation using dmol3 module in Material Studio.

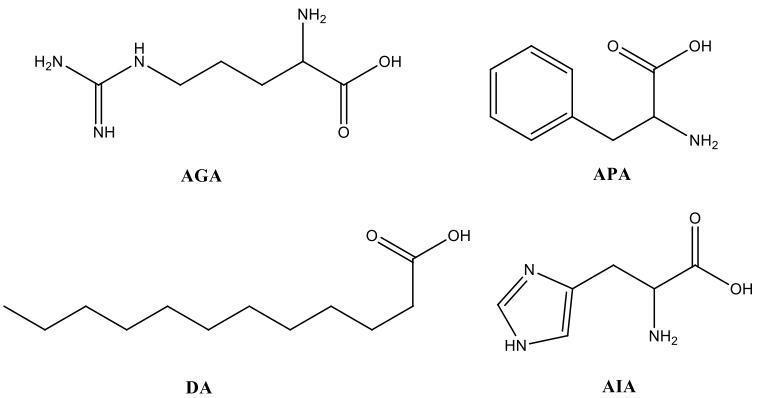

Figure 1. The main constituents of IBLE.

The geometrical optimization of these molecules in neutral (AGA, APA, DA, AIA) and protonated ($AGAH^+$, $APAH^+$, DAH^+, $AIAH^+$) states was accomplished by the GGA/BLYP method in conjunction with DNP basis set. Besides, the adsorption relationship between IBLE molecules (neutral and protonated states) and Fe substrate was calculated by MD simulation in forcite module. Fe (110) surface was used as Fe substrate. A simulation box (30.6×35.2×52.1 Å) containing 1 inhibitor molecule, 300 H_2O molecules, 5 layers Fe atoms, as well as 30 Å vacuum layer was built. The COMPASS force field, NVT canonical ensemble, and periodic boundary condition were applied in the simulation. Meanwhile, the relevant simulation time is 500 ps and time step is 1 fs.

3. RESULTS AND DISCUSSION

3.1. PDP analyses

The kinetics of anodic and cathodic reactions was investigated by the PDP measurement. The OCP-time and polarization curves of Q235 steel in 1 mol/L HCl with and without various concentrations of IBLE at 298 K are given in Fig. 2.

Table 1. PDP parameters of Q235 steel without and with IBLE at 298 K.

C (mg/L)	E_{corr} (mV/SCE)	I_{corr} (μA cm^{-2})	β_c (mV dec^{-1})	β_a (mV dec^{-1})	η (%)
Blank	−454	2.16	−140	96	–
50	−466	0.25	−136	78	88.4
100	−467	0.16	−126	73	92.6
150	−468	0.14	−132	75	93.5
200	−468	0.13	−135	75	94.0

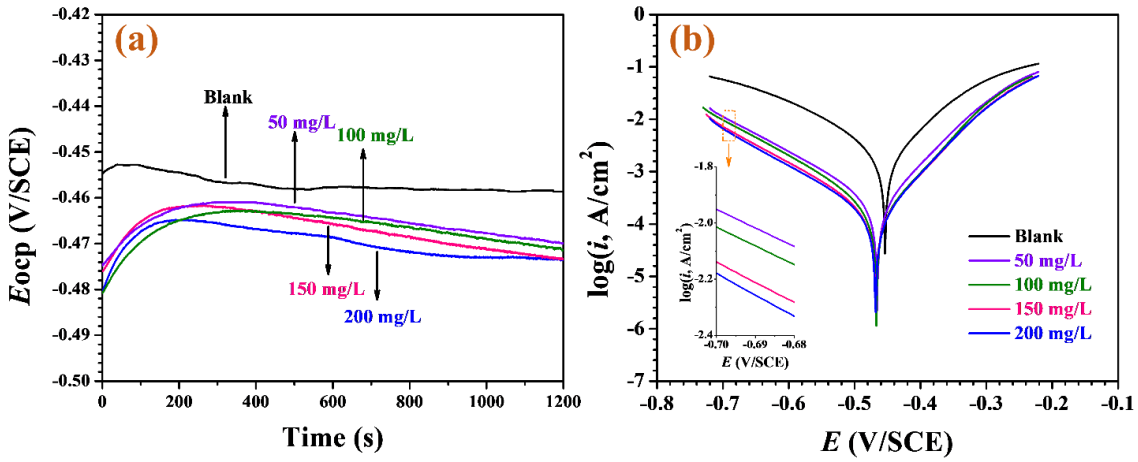

Figure 2. The (a) OCP-time and (b) PDP curves of Q235 steel immersed in 1 mol/L HCl containing various concentrations of IBLE, the inserted figure in Fig. 2b is a partial magnification.

The obtained corrosion parameters including E_{corr}, i_{corr}, cathodic and anodic Tafel slopes (β_c and β_a) are shown in Table 1. The inhibition efficiency (η) value was calculated as follows,

$$\eta = \frac{i_{corr,\,0} - i_{corr}}{i_{corr,0}} \times 100\% \qquad (1)$$

here, $i_{corr,0}$, and i_{corr} represent corrosion current densities without and with IBLE, respectively.

As seen in Fig. 2a, the *E*ocp values can reach a stable state after 1200 s immersion. It is noted that introducing IBLE inhibitor let the *E*ocp values move in the negative direction. Meanwhile, the position of PDP curves (Fig. 2b) remarkably move down in the presence of IBLE, and keep move down as increasing the IBLE concentration. This phenomenon reveals the superior inhibition ability of IBLE on steel corrosion, which can be also reflected by the changes of current density values in Table 1. In addition, it is noted than both the cathodic and anodic branches in the presence of IBLE are parallel with those without IBLE, and the β_c and β_a values shown in Table 1 are similar, indicating that the cathodic (hydrogen evolution reaction) and anodic (steel dissolution) reaction process have not been changed [26]. In particular, the suppression influence of IBLE for cathodic reaction is more obvious than anodic reaction. Furthermore, the values of E_{corr} move slightly towards more negative values as the addition of inhibitor IBLE, while the displacement of E_{corr} value is far fewer than 85 mV. This finding implies the mixed-type nature of IBLE [27]. The PDP results indicate that IBLE can provide favorable protection ability for steel in HCl solution.

3.2. EIS analysis

EIS measurement was further employed to study the corrosion behavior of mild steel immersed in HCl with and without the IBLE inhibitor. The obtained Nyquist and Bode graphs are given in Fig. 3. We can see only a single depressed semicircle in the Nyquist plot (Fig. 3a), which demonstrates that corrosion process of the steel electrode was controlled by charge transfer whatever in blank and inhibited solutions [28]. As known that such behavior is often related to the frequency dispersion because of the

roughness and heterogeneities of metal electrodes surface [29]. Obviously, with the increase of IBLE concentration, the diameter of capacitive loop arc has a increase trend, which indicates that the adsorption of IBLE on steel substrate contributes to a significant increase in charge transfer resistance. As the increase of IBLE concentration (Fig. 3b), the impedance modulus (log|Z|) and phase angle values significantly increase, indicating that higher concentration of IBLE can provide better corrosion inhibition property in HCl solution.

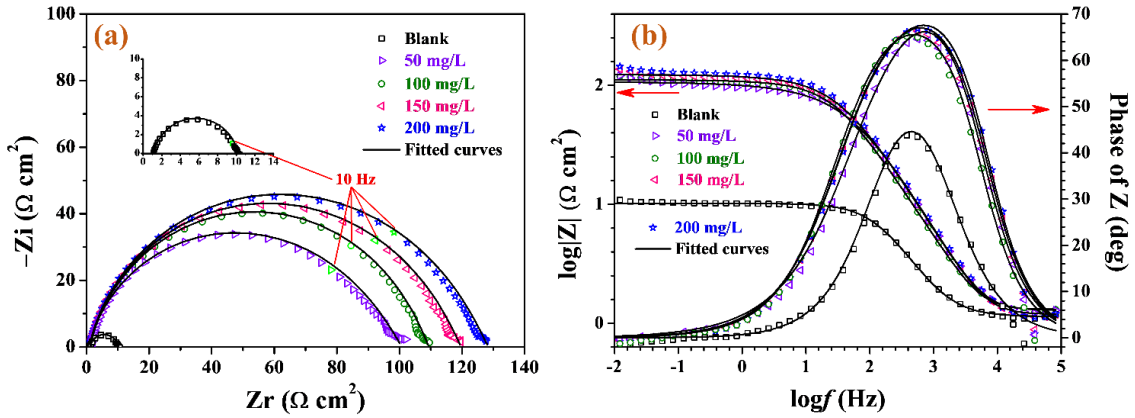

Figure 3. The (a) Nyquist and (b) Bode plots of Q235 steel immersed in HCl medium containing various concentrations of IBLE.

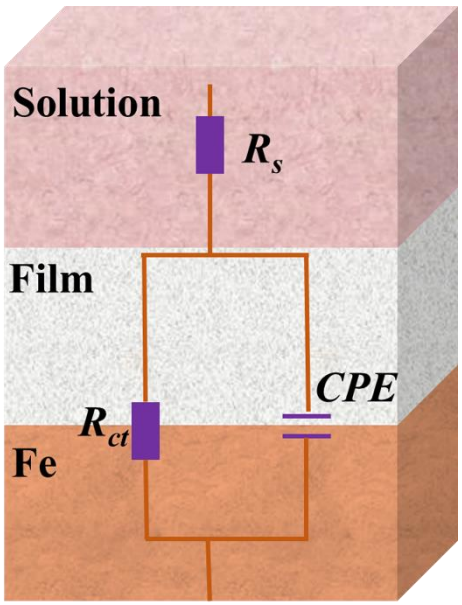

Figure 4. The equivalent circuit diagram for fitting impedance spectrum.

In order to explore the interface relationship, the equivalent circuit (Fig. 4) containing solution resistance (*R*s), charge-transfer resistance (*R*ct), and constant-phase angle element (*CPE*) was used to fit impedance spectrum data. Because the interface is not the ideal condition, the *CPE* was always used to represent electrical double-layer capacitor (C_{dl}). The η and C_{dl} can be calculated as follows [30],

$$\eta = \frac{R_{ct} - R_{ct,0}}{R_{ct}} \times 100\% \quad (2)$$

$$C_{dl} = Y_0 (w_{max})^{n-1} = Y_0 (2\pi f_{max})^{n-1} \quad (3)$$

where R_{ct} and $R_{ct,0}$ are charge-transfer resistances with and without IBLE, respectively. Y_0 is the modulus of *CPE*, w means angular frequency, the exponent n ($-1 \leq n \leq 1$) means the dispersion coefficient, and f_{max} means frequency value at the maximum imaginary component of Nyquist diagram.

Table 2. Impedance parameters of Q235 steel with and without IBLE at 298 K.

C **(mg/L)**	***R*s** **(Ω cm²)**	***R*ct** **(Ω cm²)**	***C*dl** **(μF cm⁻²)**	***n***	***η*** **(%)**
Blank	1.1	9.1	318.5	0.87	–
50	1.3	90.3	86.1	0.62	85.7
100	1.3	98.9	65.4	0.70	88.8
150	1.2	108.1	31.6	0.67	93.4
200	1.2	125.0	30.5	0.66	96.4

The obtained parameters are summarized in Table 2. As shown, the C_{dl} value decreases while R_{ct} value increases dramatically after the addition of IBLE. When the concentration of IBLE increases, this trend will continue. Compared with 9.1 Ω cm^2 for blank solution, the R_{ct} value reaches up to 125.0 Ω cm^2 at 200 mg/L, implying that IBLE can retard the steel corrosion in HCl significantly. The high C_{dl} value (318.5 μF cm^{-2}) in blank solution decreases to 30.5 μF cm^{-2} at 200 mg/L, which means the adsorption of IBLE molecules on steel substrate. A more detailed analysis can be done according to the Helmholtz model [31],

$$C_{dl} = \frac{\varepsilon^0 \varepsilon}{d} S \quad (4)$$

Where ε^0 and ε represent air and local permittivity, S stands for unprotected surface area of steel electrode, d is electric double-layer thickness. It is known that the ε value of IBLE molecule is smaller than H_2O, and the size of IBLE is larger than H_2O. Owing to the adsorption behavior of IBLE at steel electrode surface, H_2O molecules were replaced by IBLE molecules, leading to that the uncovered steel surface area and ε value decline, while the d value increases. As a result, the C_{dl} value decreases. In addition, the η value reaches up to 96.4% at 200 mg/L from 85.7% at 50 mg/L, which indicates that IBLE can provide benign inhibition performance at even low concentration.

3.3. Weight loss and Adsorption model

To further estimate the inhibition effect of IBLE, weight loss test was employed for Q235 steel in 1 M HCl at 298 K. The relevant v and η values were calculated as follows,

$$v = \frac{W_0 - W}{St} \quad (5)$$

$$\eta(\%) = \frac{v_0 - v}{v_0} \times 100 \quad (6)$$

where W_0 and W are weight of steel before and after immersion in HCl media, S means steel surface area, v_0 and v are corrosion rates without and with IBLE, respectively. The relevant results are presented in Fig. 5a. As shown, the v values remarkably decrease with the addition and higher concentration of IBLE, and thus the η values increase and exceed 90%. This contributes to the adsorption of IBLE onto steel samples, consequently forming a strong protective barrier between steel and acid solution.

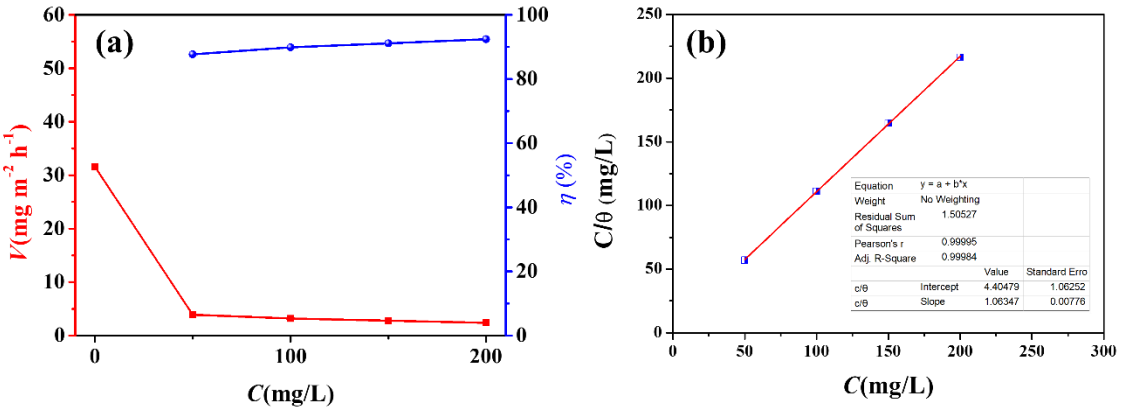

Figure 5. The (a) weight loss and (b) Langmuir plots of Q235 steel in 1 mol/L HCl with the addition of IBLE.

The adsorption isotherm was analyzed for understanding the adsorption behavior of IBLE molecules on steel. The adsorption isotherm type was determined by IBLE concentration (C) and surface coverage θ (η/100). In this study, the θ values of IBLE were obtained from weight loss results in Fig. 5a. We find that the Langmuir isotherm is the best agreement. The Langmuir adsorption isotherm is expressed by the adsorption equilibrium (K_{ads}) [32, 33],

$$\theta/(1-\theta) = K_{ads}C \qquad (7)$$

The standard adsorption free energy (ΔG^0_{ads}) value was calculated as following equation [24, 34],

$$\Delta G^0_{ads} = -RT\ln(1000K_{ads}) \qquad (8)$$

where R represent molar gas constant and T means absolute temperature. Fig. 5b shows Langmuir plot of Q235 steel in HCl with addition of IBLE. Accordingly, the key parameters K_{ads} (227.0 L/g) and ΔG^0_{ads} (−30.6 kJ/mol) were obtained respectively. The negative values of ΔG^0_{ads} reveals that IBLE molecules spontaneously adsorb onto steel surface. In general, the adsorption process can be considered chemisorption when the ΔG^0_{ads} value ≤ −40 kJ mol^{-1}, while physisorption is related to ΔG^0_{ads} ≥ −20 kJ mol^{-1} [35]. In this study, the ΔG^0_{ads} value mentioned above suggests that the adsorption of IBLE inhibitor on Q235 steel surface in HCl involves both physisorption and chemisorption.

3.4 Surface morphology

Fig. 6 shows SEM images of steel samples immersed in 1 mol/L HCl medium without and with 400 mg/L IBLE respectively at 298 K. As shown, the unprotected steel surface (Fig. 6a) was severely

corroded and rough, whereas the surface (Fig. 6b) with the protection of IBLE becomes smooth. The 3D LSCM morphologies (Fig. 7) of Q235 steel in HCl solution confirmed the SEM observation. As observed in Fig. 7a, the corroded steel surface shows many flakes and pits. After the addition of IBLE, only a few corrosion products and peaks can be seen (Fig. 7b). In addition, the surface roughness (R_a) value deceases from 1.26 μm (unprotected steel) to 0.29 μm (protected steel) in HCl solution.

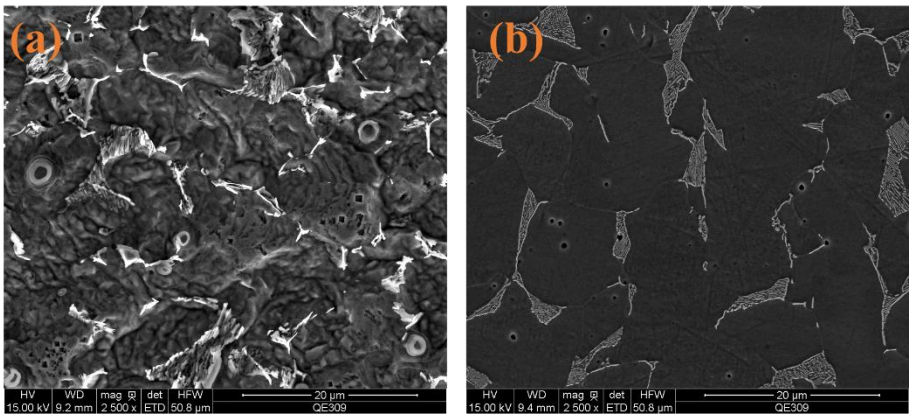

Figure 6. The SEM morphology images of steel samples immersed in 1 mol/L HCl medium without (a) and with (b) 400 mg/L IBLE after 4 h immersion.

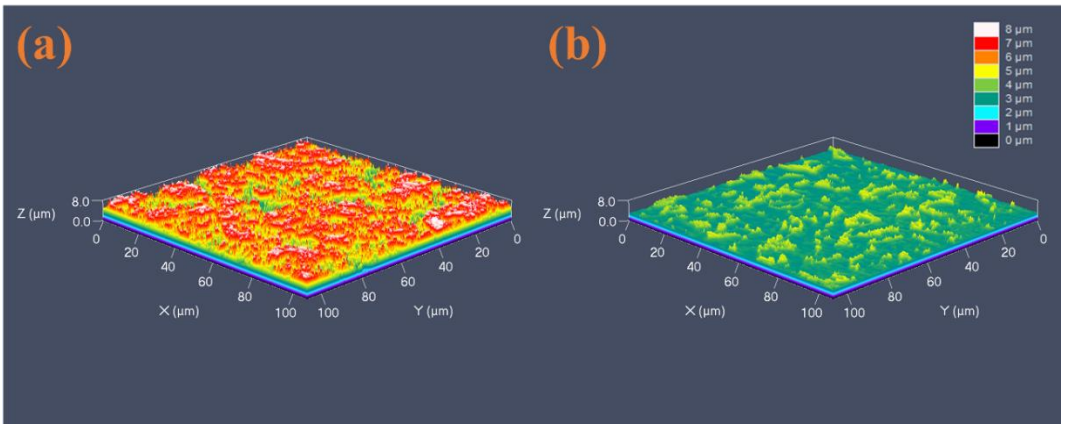

Figure 7. The LSCM images of steel samples immersed in 1 mol/L HCl medium without (a) and with (b) 400 mg/L IBLE after 1 h immersion.

In conclusion, these observations indicate that IBLE film was successfully formed on surface of Q235 steel and thus exhibits a good inhibition performance.

3.5 DFT study

In this work, the quantum chemical calculation was explored to study the interaction between steel and IBLE for both neutral and protonated forms. Consequently, the optimized structure, lowest unoccupied molecular orbital (LUMO), highest occupied molecular orbital (HOMO) distribution are

shown in Figs. 8 and 9. For neutral form of IBLE molecules (Fig. 8), the HOMO and LUMO are mainly distributed on the imidazole ring, phenyl ring, carboxyl and amino groups. In particular, the whole molecular skeleton of APA and AIA is filled with both HOMO and LUMO, which suggests that these molecules tend to adsorb onto the metal surface in parallel. As presented in Fig. 9, the protonation of these molecules influences the molecular orbital distribution to some extent. In this case, it is noted that HOMO distributes on half molecule and LUMO distributed on other half for all four molecules.

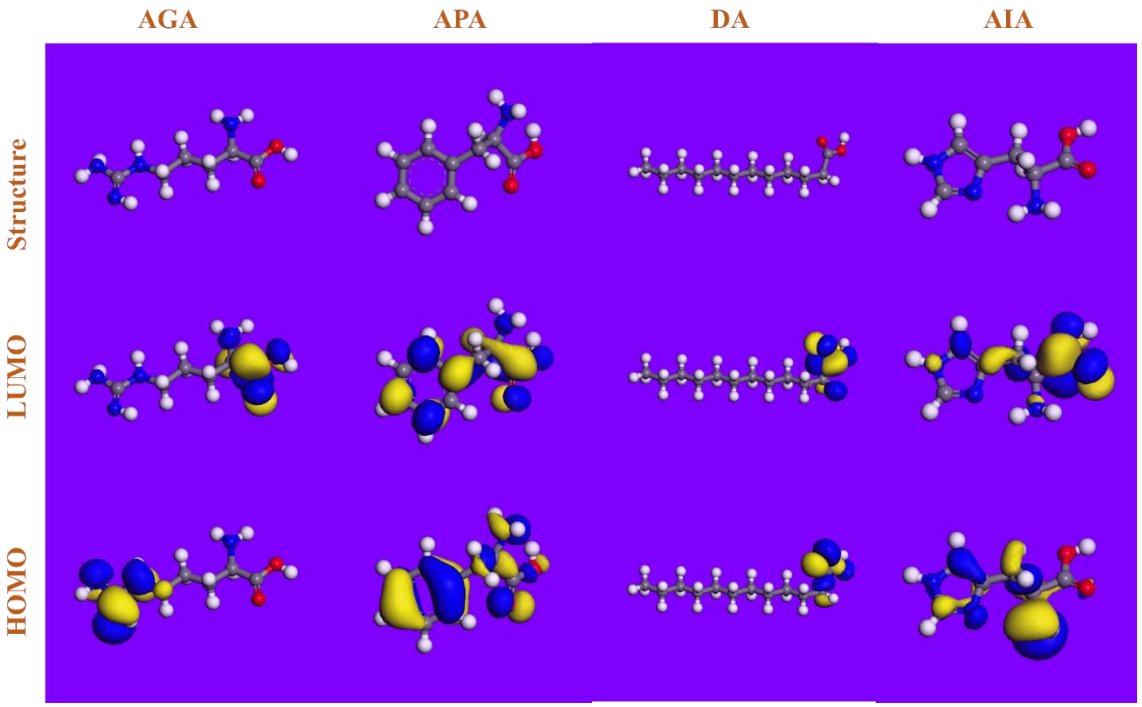

Figure 8. The optimized structures and frontier orbital (HOMO, LUMO) density distributions of main IBLE components in neutral state.

Table 3. The quantum chemical parameters for neutral and protonated organic components of IBLE.

Index	AGA	APA	DA	AIA	$AGAH^+$	$APAH^+$	DAH^+	$AIAH^+$
E_{LUMO} (eV)	–1.33	–1.08	–0.97	–1.00	–5.83	–6.14	–7.80	–5.27
E_{HOMO} (eV)	–5.22	–5.67	–6.35	–4.95	–7.73	–8.95	–8.90	–9.53
ΔE (eV)	3.89	4.59	5.38	3.95	1.90	2.81	1.10	4.26
μ (D)	4.86	4.89	1.40	5.84	21.31	30.2	56.12	16.3

The relevant quantum chemical parameters for neutral and protonated organic components of IBLE are listed in Table 3. Based on frontier orbital theory, the chemical interaction of reacting species can be dominated by E_{HOMO} and E_{LUMO} values. The higher E_{HOMO} value means stronger electrons-giving tendency, while the lower value of E_{LUMO} represents the higher electrons-receiving ability [25, 36]. Therefore, it becomes important to compare the energy gap ($\Delta E = E_{LUMO} - E_{HOMO}$) value, which means interaction ability between metal and inhibitor. The smaller value of ΔE reveals stronger interaction between reacting species, which can cause stronger adsorption strength of organic molecules onto metal substrate [37]. As shown in Table 3, AGA and DAH^+ may play a main role for inhibiting steel corrosion. In addition, the value of dipole moment (μ) is also vital to evaluate adsorption affinity of organic compounds. In general, higher μ value means higher adsorption ability [38]. As seen that the protonated form of the molecule almost exhibit the lower ΔE and higher μ value, indicating the better inhibition performance of protonated inhibitor molecules compared with the neutral form.

3.6 MD simulation

The classical MD simulation was conducted to concern the IBLE/steel intermolecular interactions at molecular level. The adsorption equilibrium configurations of AGA, APA, DA and AIAs at neutral and protonated forms on Fe (110) are visualized in Figs. 10 and 11, respectively.

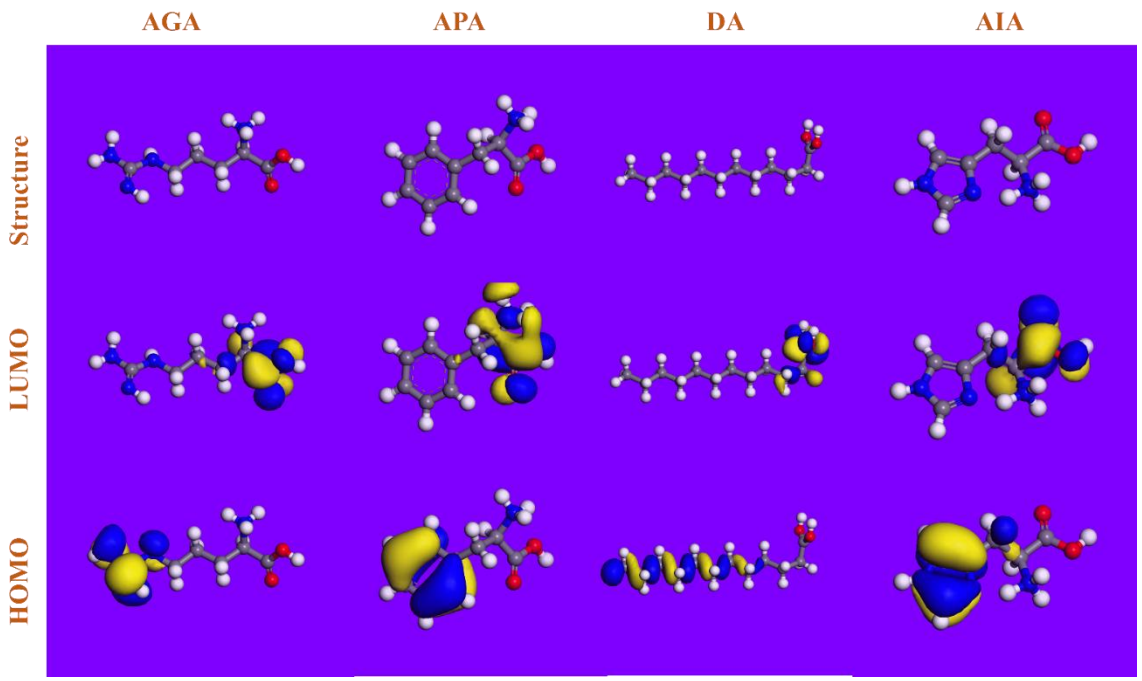

Figure 9. The optimized structures and frontier orbital (HOMO, LUMO) density distributions of main IBLE components in protonated state.

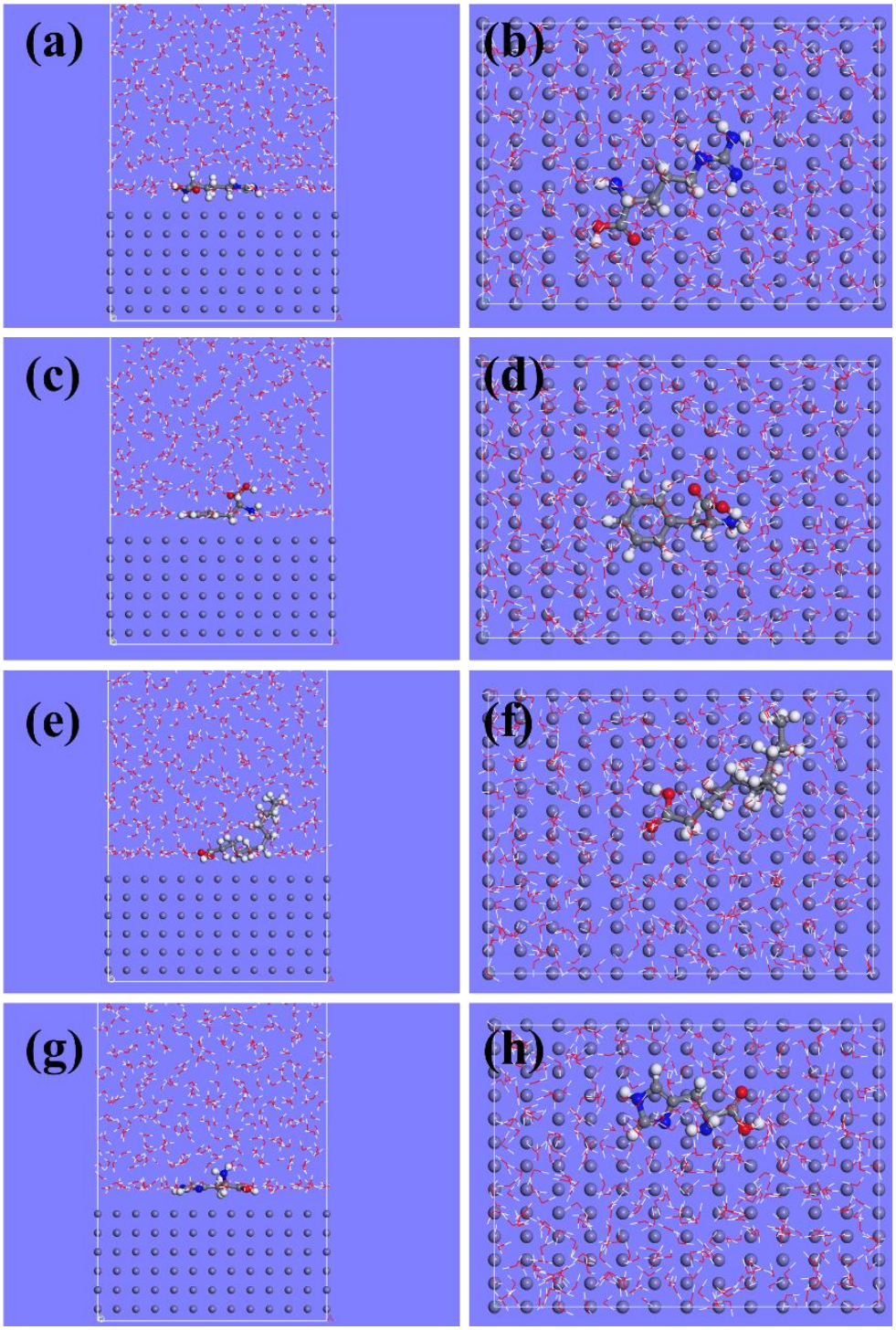

Figure 10. Equilibrium configurations of the IBLE in neutralization condition on Fe (110) surface, (a, b) AGA, (c, d) APA, (e, f) DA, (g, h) AIA.

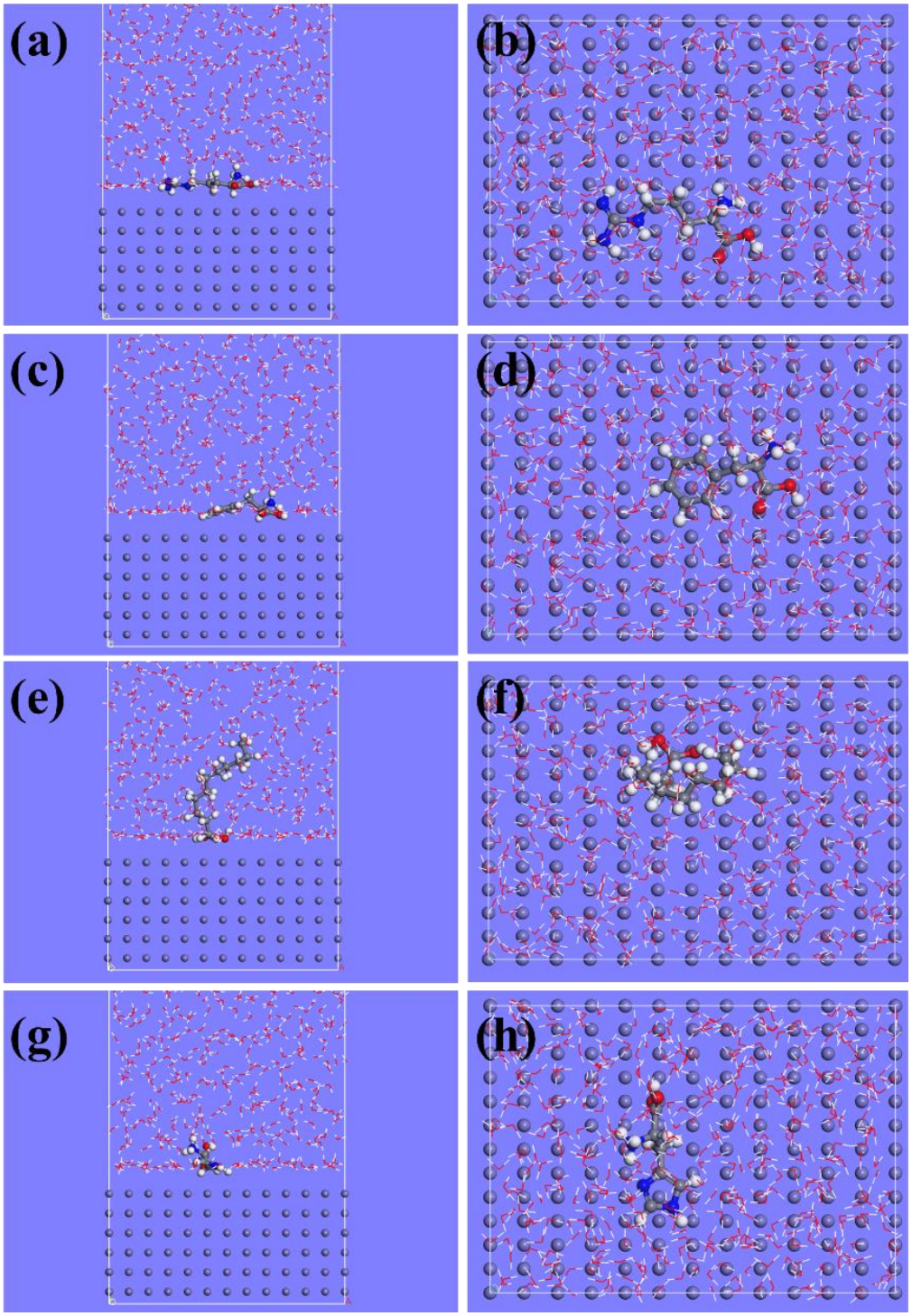

Figure 11. Equilibrium configurations of the IBLE in protonation conditions on Fe (110) surface, (a, b) $AGAH^+$, (c, d) $APAH^+$, (e, f) DAH^+, (g, h) $AIAH^+$.

Both side and top views reflect that all these green substances align parallel with respect to Fe surface. Particularly, it is noted that DA molecule paralleled adsorbed onto Fe substrate with a vertical alkyl chain, which can provide a hydrophobic property. Furtherly, the main MD index including interaction energy ($E_{interact}$), binding energy ($E_{binding}$) of neutral and protonated organic components of IBLE on Fe(110) surface were calculated [39] and shown in Table 4.

Table 4. The MD index of neutral and protonated organic components of IBLE on Fe(110) surface.

Energy(kcal/mol)	AGA	APA	DA	AIA	$AGAH^+$	$APAH^+$	DAH^+	$AIAH^+$
$E_{interact}$	–149.3	–107.2	–93.0	–120.1	–239.2	–219.0	–78.7	–173.2
$E_{binding}$	149.3	107.2	93.0	120.1	239.2	219.0	78.7	173.2

The $E_{binding}$ values of AGA at two forms are higher than other green substances, indicating the stronger attachment of AGA and $AGAH^+$ to steel substrate. These modeling observation reveals the affinity of these molecules onto Fe(110) surface, demonstrating the green inhibitors protective capability for steel against corrosive attack, which agrees well with experimental results above.

4. CONCLUSION

The corrosion inhibition of IBLE for Q235 steel in 1 M HCl solution was investigated through experimental and computational (MD, DFT) techniques. The obtained conclusions are listed as follows:

(1) Experimental and theoretical methods reveal that IBLE is a high-efficiency corrosion inhibitor for Q235 steel in HCl medium. The optimal inhibition efficiency can achieve about 96.4% at 200 mg/L.

(2) From PDP measurements, it is found that IBLE acts as a mixed-type inhibitor. It influences both anodic and cathodic electrochemical reactions.

(3) SEM and LSCM morphology observations demonstrate that IBLE molecules adsorbed onto the steel surface to form a protective film, which protected steel substrate from the corrosive attacks.

(4) DFT calculation indicates that IBLE molecules contain highly reactive sites which are the sources of their inhibition performance. In addition, MD simulation reveals that IBLE molecules spontaneously and strongly adsorb onto the Fe(110) surface with parallel state.

DECLARATION OF COMPETING INTEREST

The authors declared that they have no conflicts of interest to this work.

References

1. I. Martinović, G.Z. Zora Pilić, L. Šušić, O. Kowalska, D. Petrović, F. Falak, and J. Mišković, *Int. J. Electrochem. Sci.,* 14 (2019) 4206.
2. Y. Ji, B. Xu, W. Gong, X. Zhang, X. Jin, W. Ning, Y. Meng, W. Yang, Y. Chen, *J. Taiwan Inst. Chem. E.*, 66 (2016) 301-312.
3. Y. Qiang, L. Guo, S. Zhang, W. Li, S. Yu, J. Tan, *Sci. Rep.*, 6 (2016) 33305.
4. Y. Qiang, S. Zhang, S. Xu, L. Guo, N. Chen, I.B. Obot, *Inter. J. Electrochem. Sci.*, 11 (2016) 3147.
5. B. Tan, S. Zhang, Y. Qiang, L. Feng, C. Liao, Y. Xu, S. Chen, *J. Mol. Liq.*, 248 (2017) 902-910.

6. Y. Qiang, L. Guo, H. Li, X. Lan, *Chem. Eng. J.*, 406 (2021) 126863.
7. M. Cui, S. Ren, H. Zhao, L. Wang, Q. Xue, *Appl. Surf. Sci.*, 443 (2018) 145-156.
8. Y. Qiang, S. Zhang, H. Zhao, B. Tan, L. Wang, *Corros. Sci.*, 161 (2019) 108193.
9. Y. Qiang, S. Zhang, L. Guo, X. Zheng, B. Xiang, S. Chen, *Corros. Sci.*, 119 (2017) 68-78.
10. C. Verma, I.B. Obot, I. Bahadur, E.-S.M. Sherif, E.E. Ebenso, *Appl. Surf. Sci.*, 457 (2018) 134-149.
11. Y. Guo, B. Xu, Y. Liu, W. Yang, X. Yin, Y. Chen, J. Le, Z. Chen, *J. Ind. Eng. Chem.*, 56 (2017) 234-247.
12. J. Du, Y. Liu, P. Liu, Y. Liu, S. Gao, and L. Zhang, *Int. J. Electrochem. Sci.*, 14 (2019) 4532.
13. Y. Qiang, S. Zhang, B. Tan, S. Chen, *Corros. Sci.*, 133 (2018) 6-16.
14. B. Tan, B. Xiang, S. Zhang, Y. Qiang, L. Xu, S. Chen, J. He, *J. Colloid Interf. Sci.*, 582 (2021) 918-931.
15. X. Zuo, W. Li, W. Luo, X. Zhang, Y. Qiang, J. Zhang, H. Li, B. Tan, *J. Mol. Liq.*, 321 (2021) 114914.
16. M. Prabakaran, S.-H. Kim, V. Hemapriya, I.-M. Chung, *J. Ind. Eng. Chem.*, 37 (2016) 47-56.
17. H. Li, S. Zhang, Y. Qiang, *J. Mol. Liq.*, 321 (2021) 114450.
18. M. Motamedi, B. Ramezanzadeh, M. Mahdavian, *J. Ind. Eng. Chem.*, 66 (2018) 116-125.
19. A. Dehghani, G. Bahlakeh, B. Ramezanzadeh, M. Ramezanzadeh, *J. Taiwan Inst. Chem. E.*, 102 (2019) 349-377.
20. M. Mobin, M. Basik, M. Shoeb, *Appl. Surf. Sci.*, 469 (2019) 387-403.
21. M. Ramezanzadeh, G. Bahlakeh, B. Ramezanzadeh, *J. Mol. Liq.*, 292 (2019) 111387.
22. Z. Sanaei, G. Bahlakeh, B. Ramezanzadeh, M. Ramezanzadeh, *J. Mol. Liq.*, 290 (2019) 111176.
23. S. Chen, S. Chen, B. Zhu, C. Huang, W. Li, *J. Mol. Liq.*, 311 (2020) 113312.
24. P.E. Alvarez, M.V. Fiori-Bimbi, A. Neske, S.A. Brandán, C.A. Gervasi, *J. Ind. Eng. Chem.*, 58 (2018) 92-99.
25. M. Ramezanzadeh, G. Bahlakeh, Z. Sanaei, B. Ramezanzadeh, *Appl. Surf. Sci.*, 463 (2019) 1058-1077.
26. Y. Qiang, H. Li, X. Lan, *J. Mater. Sci. Technol.*, 52 (2020) 63-71.
27. Y. Qiang, S. Zhang, L. Guo, S. Xu, L. Feng, I.B. Obot, S. Chen, *J. Clean. Prod.*, 152 (2017) 17-25.
28. S. Y. Al-Nami, *Int. J. Electrochem. Sci.*, 14 (2019) 3986.
29. Y. Qiang, S. Zhang, S. Yan, X. Zou, S. Chen, *Corros. Sci.*, 126 (2017) 295-304.
30. Z. Wang, Y. Gong, C. Jing, H. Huang, H. Li, S. Zhang, F. Gao, *Corros. Sci.*, 113 (2016) 64-77.
31. L. Hu, S. Zhang, W. Li, B. Hou, *Corros. Sci.*, 52 (2010) 2891-2896.
32. J. Haque, K.R. Ansari, V. Srivastava, M.A. Quraishi, I.B. Obot, *J. Ind. Eng. Chem.*, 49 (2017) 176-188.
33. H. Li, Y. Qiang, W. Zhao, S. Zhang, *Corros. Sci.*, 191 (2021) 109715.
34. M. Prabakaran, S.-H. Kim, N. Mugila, V. Hemapriya, K. Parameswari, S. Chitra, I.-M. Chung, *J. Ind. Eng. Chem.*, 52 (2017) 235-242.
35. Y. Qiang, S. Zhang, L. Wang, *Appl. Surf. Sci.*, 492 (2019) 228-238.
36. M. Ramezanzadeh, G. Bahlakeh, B. Ramezanzadeh, Z. Sanaei, *J. Ind. Eng. Chem.*, 77 (2019) 323-343.
37. Y. Qiang, S. Zhang, S. Xu, W. Li, *J. Colloid Interf. Sci.*, 472 (2016) 52-59.
38. L. Guo, S. Kaya, I.B. Obot, X. Zheng, Y. Qiang, *J. Colloid Interf. Sci.*, 506 (2017) 478-485.
39. H. Li, S. Zhang, B. Tan, Y. Qiang, W. Li, S. Chen, L. Guo, *J. Mol. Liq.*, 305 (2020) 112789.